Quantum description of the optical response of charged monolayer–thick metallic patch nanoantennas

Mario Zapata Herrera, Andrey K. Kazansky, Javier Aizpurua, and Andrei G. Borisov

Phys. Rev. B **95**, 245413 — Published 12 June 2017

DOI: 10.1103/PhysRevB.95.245413

Quantum description of the optical response of charged monolayer-thick metallic patch nanoantennas

Mario Zapata Herrera,[1,2] Andrey K. Kazansky,[1,3] Javier Aizpurua,[2,1] and Andrei G. Borisov[4]

[1] *Donostia International Physics Center DIPC, Paseo Manuel de Lardizabal 4 20018, Donostia-San Sebastían, Spain*
[2] *Materials Physics Center CSIC-UPV/EHU, Paseo Manuel de Lardizabal 5 20018, Donostia-San Sebastián Spain*
[3] *IKERBASQUE, Basque Foundation for Science, 48013 Bilbao, Spain*
[4] *Institut des Sciences Moléculaires d'Orsay ISMO, UMR 8214 CNRS-Université Paris-Sud, Bât. 351, Université Paris-Sud, 91405 Orsay Cedex, France**

(Dated: May 22, 2017)

The optical response of small charged metallic nanodisks of one atomic monolayer thickness is analysed under the excitation by an incident plane wave and by a localised point-like dipole. Using the time-dependent density functional theory (TDDFT) and classical electrodynamical calculations we identify the bright and dark plasmon modes and study their evolution under external charging of the nanostructure. For neutral nanodisks, despite their monolayer thickness, the in-plane optical response, as obtained from TDDFT, is in agreement with classical electromagnetic results. The optical response for an incident wave polarised perpendicular to the nanostructure cannot be retrieved classically as it reflects a discrete energy structure of electronic levels. This latter situation appears most sensitive to external charging while the energy of the in-plane plasmon with dipolar character is nearly charge-independent.

I. INTRODUCTION

The ability to manipulate and confine light well below the diffraction limit as offered by metallic plasmonic structures[1] allows for a wealth of practical applications from bio-sensing[2] and optical nanoantennas[3,4] to plasmon-enhanced photodetection[2,5–8], photochemistry[9,10], nonlinear optics[11,12], and energy harvesting[10,13]. Nowadays, plasmonic devices exploit propagating plasmons confined to (nanostructured) metal surfaces, or localised plasmons in single nanoparticles and nanoparticle assemblies. Along with these three-dimensional structures, plasmonics in lower dimensional structures such as nanowires[14–18] or edges[19–25] or two-dimensional materials[23–29] offers further perspectives in miniaturization of optoelectronic devices, light confinement, active control of response, and directional plasmon propagation. Albeit the ongoing discussion on the applicability of the term "plasmonic" to describe optical resonances in molecular structures, these structures represent the smallest devices where the optical response reflects the quantum nature of collective electronic excitations and thus requires quantum description[30–32].

Plasmonics in the nanostructures where one or several dimensions are in the nm range rises an important practical issue concerning interpretation and prediction of the optical properties. Indeed, classical approaches based on Maxwell equations with the use of local dielectric functions to describe the materials properties allow complete characterization of the interaction of light with systems of basically any shape and composition. These classical results are thus extremely valuable to guide the design and fabrication of plasmonic devices with sought optical properties. On the other hand, when one or more dimension(s) of the structure becomes very small, classical descriptions might not be completely adequate and need to be applied with care. The quantum effects such as quantization of the electron motion, the spill out of the electron density outside the geometrical boundary and the tunneling across a narrow junction become important[33–40]. In this context, understanding of the quantum/classical correspondences in individual and coupled plasmonic systems when they are subjected to external perturbations allows to develop efficient strategies of the active control. Indeed, active control of the plasmonic modes by applied dc fields[42–46] or charging[47–50] has been reported in the literature. In particular, if possible for metallic nanostructures[51,52], the plasmon frequency change via electron doping as known in the THz range for semiconductor quantum wells or graphene[26–29,53–55] would allow active ultracompact devices in the visible range. Metals, however represent a challenge because of the high density of conduction electrons and thus of the high levels of charging needed to reach observable effects.

To address the properties and limitations of low-dimensional plasmonics with standard metals, in this work we study bright and dark breathing plasmon modes in free-electron metal nanodisks with a thickness of a single atomic layer (1 monolayer, 1 ML), using the self-consistent density functional theory (DFT), time-dependent density functional theory (TDDFT), and classical electromagnetic calculations. Particular emphasis is given to the dependence of the optical response on the external charging of the nanostructure with the perspective to reveal the possibility of its active control. We show that for a neutral disk, despite its 1 ML thickness, classical electromagnetic theory correctly reproduces the quantum results for in-plane plasmon modes characterized by the distribution of the charge density symmetric with respect to the equatorial plane of the disk. In

contrast, the optical excitations associated with antisymmetric induced charge distribution require transitions between quantized electronic states perpendicular to the disk plane and cannot be retrieved classically. For negatively charged nanodisks we show that because of the quantum confinement of the electron motion perpendicular to the disk plane, and because of the electron density spill out, the frequency shifts of the plasmon modes induced by the external charging are generally not captured by the classical theory. Our work demonstrates the existence of "quantum" and "classical" degrees of freedom in low dimensional structures and establishes quantum limits to the possibility of active control of plasmon modes in 2D metal structures via charge carrier injection.

The paper is organized as follows. First, we describe the geometry of the system under study, the free electron model of the metal, and the calculation methods used to obtain the optical response. We show our results and discuss them in the next sections, addressing the ground state properties of neutral and externally-charged nanodisks, and presenting a detailed analysis of the optical response and plasmon modes of the nanodisks excited by an incident plane wave and by a point dipole. The conclusions and outlook section closes the paper. Unless otherwise stated, atomic units are used throughout the paper.

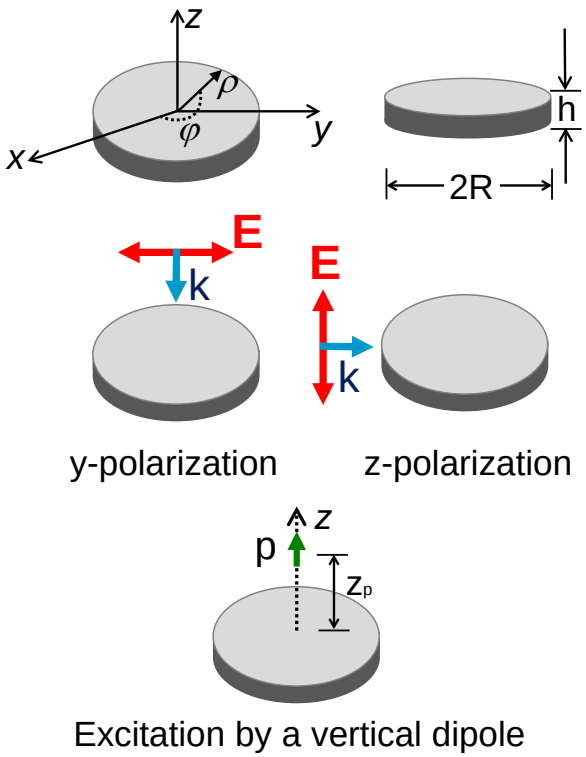

FIG. 1. Schematics of the model systems used in the calculations. Upper panels present the nanodisk geometry characterized by a radius $R = 42.7$ Å with a monolayer thickness $h = 2.1$ Å, corresponding to the sodium metal. The neutral system comprises 304 electrons. For the calculations we use a cylindrical coordinates system $\mathbf{r} = (\rho, \varphi, z)$ with $z = 0$ placed in the middle of the disk. Middle panels show two different polarizations of the plane wave incident at the nanostructure. $\mathbf{E}$ is the electric field and $\mathbf{k}$ is the photon momentum. The lower panel represents the excitation of the dark breathing plasmon modes by a vertical point dipole $\mathbf{p}$ placed along the symmetry axis z, at position z_p above the disk.

II. SYSTEM AND COMPUTATIONAL ASPECTS

A. Model system

The sketch of the free-electron metal nanodisk in vacuum used in our study is shown in Fig. 1 together with the different types of plasmon excitation considered. The nanodisk is described within the jellium metal (JM) approximation[56], well suited for studying the collective behaviour of conduction electrons in nanostructures[33,57–60]. Within the JM, the positive ion cores at the lattice sites are not treated explicitly but represented by a uniform background density $n_+ = (4\pi r_s^3/3)^{-1}$ confined within the jellium edges that define the geometrical surface of the nanoparticle. A Wigner-Seitz radius $r_s = 4$ a$_0$, characteristic of the Na metal, is used (a$_0 = 0.53$ Å is the Bohr radius). Together with Al, recently placed at the focus of research in plasmonics[61,62], Na is a prototype of a free electron metal[63], and it allows to address plasmon resonances within a frequency range similar to that of silver and gold nanoparticles. The neutral system comprises $N_e = 304$ electrons and has a height $h = 3.99$ a$_0$ (2.1 Å) corresponding to the spacing between atomic planes of the Na(100) surface[64]. Similar to graphene structures, we consider the case of a nanodisk formed by a single layer (1ML) of atoms. The radius of the disk is thus $R = (N_e/\pi h n_+)^{1/2} = 80.627$ a$_0$ (42.7 Å). It is worth to mention that despite its simplicity, the JM allowed semi-quantitative predictions of many interesting physical phenomena in subnanometric plasmonics, such as the evolution of plasmon resonances in metallic nanoclusters and nanoshells[33,57,60], or tunneling effects in narrow plasmonic gaps[38,39,65]. The conclusions derived from the JM calculations have been later confirmed by the experimental data[40,66–69], and ab-initio calculations at a full atomistic level[70–72].

To capture the dynamics of bright and dark plasmon modes in the system we have considered different types of excitation: an incident linearly polarized electromagnetic plane wave and a point dipole, as indicated in the lower panels of Fig. 1. The incident plane wave polarised along the y-axis allows to probe the optical response of the nanodisk in the in-plane direction. Here, owing to the relatively large radius of the disk R, a quasi-continuum of electronic states is formed leading to a well developed dipolar plasmon. The incident plane wave polarised along the z-axis allows to probe the system in the "quan-

tum" direction. Indeed, as we show below, because of the nanodisk thickness of a few Ångstroms, the discrete structure of electron energy levels determines the optical response for the z-polarized light. Finally, with a vertical dipole, $\mathbf{p}$, located on the symmetry z-axis above the center of the disk (lower panel of Fig. 1) at position $z = z_p$, the breathing dark plasmon modes[73] are excited.

B. DFT and TDDFT calculations

Prior to the implementation of the TDDFT calculations of the optical response of our system, the ground state properties of the neutral and charged nanoparticle are obtained within the Kohn-Sham (KS) scheme of DFT[74]. In short, the electron density of the system is given by

$$n(\mathbf{r}) = \sum_j F(E_j - E_F) \left|\psi_j^{gs}(\mathbf{r})\right|^2, \quad (1)$$

where the sum runs over the KS orbitals $\psi_j^{gs}(\mathbf{r})$ with energies E_j, assuming equal occupation of the "up" and "down" spin states. The superscript gs stands for the ground state. To accelerate the convergence of the DFT calculations, a small energy broadening given by the Fermi distribution function $F(E_j - E_F)$ with temperature $T = 290$ K is introduced (E_F stands for the Fermi energy). The wave functions $\psi_j^{gs}(\mathbf{r})$ and their energies E_j are obtained from the solution of the stationary Schrödinger equation

$$\left[\hat{T} + V_{\rm xc}(n,\mathbf{r}) + V_{\rm H}(n,\mathbf{r})\right] \psi_j^{gs}(\mathbf{r}) = E_j \psi_j^{gs}(\mathbf{r}). \quad (2)$$

In Eq. (2), $\hat{T}$ stands for the kinetic energy operator, $V_{\rm xc}(n,\mathbf{r})$ is the exchange-correlation potential derived within the local density approximation (LDA) from the exchange-correlation functional of Gunnarson and Lundqvist[75], and $V_{\rm H}(n,\mathbf{r})$ is the Hartree potential. We use cylindrical coordinates, $\mathbf{r} = (\rho,\varphi,z)$, as shown in Fig. 1. With wave functions $\psi_j^{gs}(\mathbf{r})$ sought in the form $\psi_j^{gs}(\mathbf{r}) = \exp[iM\varphi]\ \tilde{\psi}_f(\rho,z)$, Eq. (2) is then solved separately for each M subspace on a (ρ,z) mesh. The M and f quantum numbers are thus grouped in j.

The electron density dynamics triggered by an external perturbation in neutral and charged nanodisks is calculated using the real time propagation within the TDDFT[76,77]. The time-dependent KS equations

$$i\frac{\partial \psi_j(\mathbf{r},t)}{\partial t} = V(\mathbf{r},t)\psi_j(\mathbf{r},t) \quad (3)$$

are solved on a mesh in cylindrical coordinates with initial condition $\psi_j(\mathbf{r},t=0) = \psi_j^{gs}(\mathbf{r})$. The specific numerical implementation of our approach is detailed elsewhere[39]. In Eq. (3), $V(\mathbf{r},t)$ is a time-dependent effective one-electron potential given by the sum of the exchange-correlation, Hartree, and external potential contributions:

$$V(\mathbf{r},t) = V_{\rm xc}(n,\mathbf{r},t) + V_{\rm H}(n,\mathbf{r},t) + V_{\rm ext}(\mathbf{r},t). \quad (4)$$

We use the adiabatic local density approximation (ALDA)[76] so that the exchange-correlation potential $V_{\rm xc}(n,\mathbf{r},t)$ has the same functional dependence on the local electron density as in the DFT study. The Hartree potential $V_{\rm H}(n,\mathbf{r},t)$ is calculated from the time-dependent electron density $n(\mathbf{r},t) = \sum_j F(E_j - E_F)\left|\psi_j(\mathbf{r},t)\right|^2$, using the non-retarded approximation well suited here because of the small size of the system. Finally, $V_{\rm ext}(\mathbf{r},t)$ is the potential given by the external perturbation allowing to "probe" the electronic excitations.

We consider an impulsive perturbation with electric field polarised along the $s = x,y,z$ axis, $V_{\rm ext} = \kappa\,(\hat{e}_s\mathbf{r})\,\delta(t)$, where κ is a small constant, and $\hat{e}_s$ is the unit length vector along s-direction. The frequency-resolved absorption cross-section $\sigma_s(\omega)$ can be obtained in this case from:

$$\sigma_s(\omega) = \frac{4\pi\omega}{c}{\rm Im}\left\{\alpha_s(\omega)\right\}, \quad (5)$$

where c is the speed of light in vacuum, and the frequency-resolved dipolar polarizability of the system is calculated from the dynamics of the induced dipole using the time-to-frequency Fourier transform

$$\alpha_s(\omega) = \frac{1}{\kappa}\int_0^\infty e^{i\omega t - \eta t}dt \int_V (\hat{e}_s\mathbf{r})\, n(\mathbf{r},t) d^3\mathbf{r}. \quad (6)$$

The broadening $\eta = 0.15$ eV is introduced here to account for the various plasmon damping mechanisms beyond the TDDFT[38].

To analyse the dark plasmon modes of the nanodisk we also use an impulsive perturbation corresponding to the potential created by a point dipole, $\mathbf{p} = \hat{e}_z p$, located at the symmetry axis of the disk. In this case $V_{\rm ext} = p\frac{z-z_p}{|\mathbf{r}-\mathbf{r}_p|^3}\delta(t)$, where the dipole position vector $\mathbf{r}_p = \hat{e}_z z_p$. From the TDDFT calculations, we perform the time-to-frequency Fourier transform and obtain the normalized rate of energy dissipation by the point emitter in the presence of the nanostructure, so-called Purcell factor:[78,79]

$$\frac{P}{P_0} = 1 + \frac{3}{2p}\frac{1}{k^3} Im\left\{\hat{e}_z \mathbf{E}_{\rm ns}(\mathbf{r}_p,\omega)\right\}. \quad (7)$$

Here $\mathbf{E}_{\rm ns}(\mathbf{r}_p,\omega)$ is the frequency resolved electric field induced by the nanostructure at the dipole position, k is the photon wave vector, and P_0 is the energy dissipation rate of the point emitter in vacuum.

The total field created by the dipole placed in vicinity of the nanodisk can be expressed as

$$\begin{aligned}\mathbf{E}_{\rm tot}(\mathbf{r},\omega) &= \mathbf{E}_0(\mathbf{r},\omega) + \mathbf{E}_{\rm ns}(\mathbf{r},\omega) \\ &= \frac{4\pi}{c}\left[\mathbf{G}_0(\mathbf{r},\mathbf{r}_p,\omega) + \mathbf{G}_{\rm ns}(\mathbf{r},\mathbf{r}_p,\omega)\right]\mathbf{p}, \quad (8)\end{aligned}$$

where $\mathbf{G}_0$ is the free-space Green's dyadic and $\mathbf{G}_{\rm ns}$ is the change of the Green's dyadic because of the presence of the nanostructure. Then Eq. (7) takes the form[80,81]

$$\frac{P}{P_0} = 1 + \frac{6\pi c}{\omega} Im\left\{\hat{e}_z \mathbf{G}_{\rm ns}(\mathbf{r}_p, \mathbf{r}_p, \omega)\hat{e}_z\right\} = 1 + \frac{3\pi^2 c^3}{\omega^2}\,\mathfrak{N}_{\rm ns}(\mathbf{r}_p, \omega). \quad (9)$$

The change in the projected local electromagnetic density of states (LDOS) induced by the nanostructure, $\mathfrak{N}_{\rm ns}(\mathbf{r}_p, \omega)$, can be thus obtained from the TDDFT results using Eq. (7) and Eq. (9) as

$$\mathfrak{N}_{\rm ns}(\mathbf{r}_p, \omega) = \frac{1}{2\pi^2\omega} Im\left\{\hat{e}_z \mathbf{E}_{\rm ns}(\mathbf{r}_p, \omega)\right\}. \quad (10)$$

The frequency resolved electric field $\mathbf{E}_{\rm ns}(z_p, \omega)$ is obtained from the time-dependent Hartree field $\mathbf{E}_{\rm ns}(\mathbf{r}_p, t) = \nabla V_{\rm H}(n, \mathbf{r}_p, t)$ using time-to-frequency Fourier transform similar to Eq. (6). The dark breathing plasmon modes of the nanodisk appear as resonances in $\mathfrak{N}_{\rm ns}(\mathbf{r}_p, \omega)$, allowing the analysis of their frequencies and lifetimes.

In order to reveal the importance of quantum effects in the optical response of the system we compare the TDDFT results with those obtained using classical electromagnetic theory calculations as implemented in boundary elements method[82]. To this end, we describe the disk material by means of a local Drude dielectric function

$$\varepsilon(\omega) = 1 - \frac{\omega_p^2}{\omega(\omega + i\gamma)} \quad (11)$$

well suited for the free electron metal. Here $\omega_p = \sqrt{4\pi n_e} = 5.89$ eV is the bulk plasma frequency of Na, and $\gamma = 0.15$ eV is the corresponding damping factor due to intrinsic losses. $n_e = n_+ = \left(\frac{4\pi}{r} r_s^3\right)^{-1}$ is the density of the homogeneous free-electron gas characterised by r_s. In practice, to match the in-plane dipolar plasmon resonance frequency calculated with TDDFT for the neutral nanodisk with that obtained from classical calculations for the same electron density, we used a slightly lower value for ω_p (5.6 eV). This allows to partially account for the quantum spill out effect. For charged nanodisks, the homogeneous distribution of the extra-charges over the metal nanoparticle in the classical calculations has been assumed following standard approaches[26–28,47–52], which results in rescaling of the plasma frequency in Eq. (11) as $\omega_p \to \omega_p\sqrt{(N_e + Q)/N_e}$. Here, Q is the number of electrons added to initially neutral system.

III. GROUND STATE PROPERTIES OF MONOATOMIC METALLIC NANODISKS

A. Neutral system

In Fig. 2 we show the effective one-electron potential and ground state electronic density for the neutral nanodisk as obtained from the DFT calculations. The 1 ML

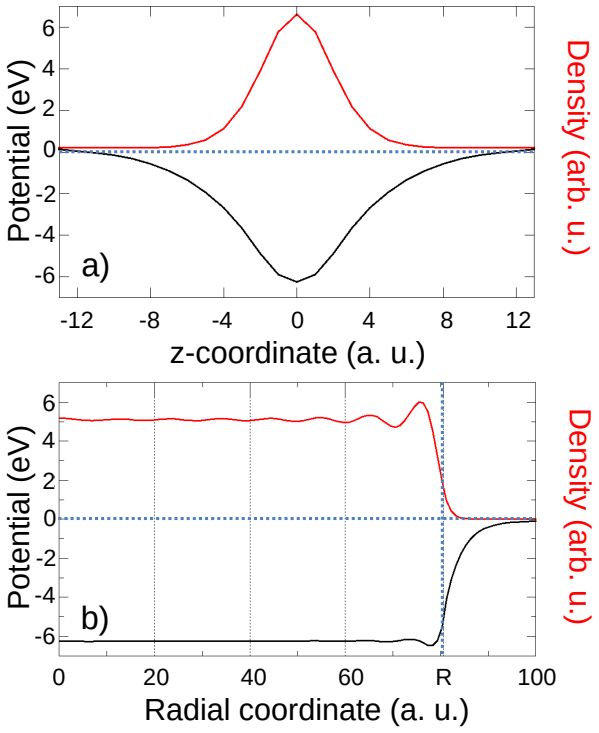

FIG. 2. Ground state electronic density (red) and one-electron effective potential (black) in a neutral sodium nanodisk calculated with DFT. a) Results along the symmetry axis of the disk are shown as a function of the $z-$coordinate. b) Results in the $z = 0$ plane (at the middle of the sodium layer) are shown as a function of the radial coordinate measured from the center of the disk. The dashed blue vertical line indicates the sodium disk boundary (jellium edge), located at $R = 80.63$ a$_0$ $= 4.26$ nm. The dashed horizontal blue line indicates the position of the vacuum level.

thickness of the nanodisk results in a narrow potential well in the direction perpendicular to its surface. To understand the distribution of energies of the electronic states associated with this system, let us consider an infinite metallic layer. In the present conditions, a single occupied state with energy E_0 exists for the electron motion in the z-direction. This state corresponds to a wave function symmetric with respect to $z = 0$. The in-plane motion in an infinite layer is free with momentum $k_\parallel$, giving rise to a continuum of occupied electronic states $E_{k_\parallel} = E_0 + k_\parallel^2/2$. Due to the finite size of the disk structure, the motion along the ρ coordinate is quantized by the reflection at the radial boundary of the disk at $\rho = R$. Neglecting the coupling of modes along the z and ρ directions at the edges, the one-electron KS orbitals of the disk form an energy sequence $E_j = E_0 + E_j^\rho$, $j = 1, 2, ...$ where E_j^ρ stands for the discrete energy values because of the quantization of the in-plane continuum. The work function of the nanodisk is $\Phi = 3.067$ eV, and the lowest KS orbital has an energy $E_1 = -4.32$ eV, as calculated here with DFT. The narrow symmetric density profile

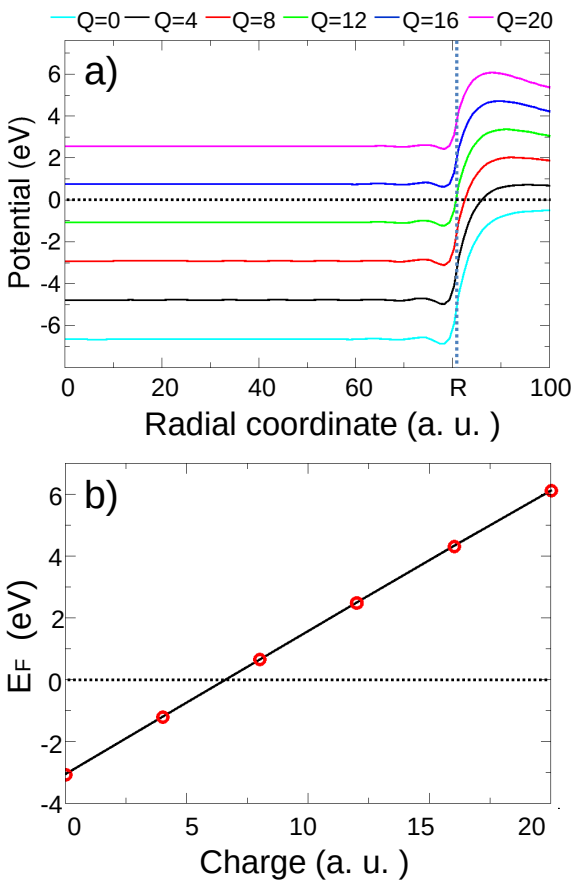

FIG. 3. Effect of extra charge on the electronic structure of a nanodisk. a) Evolution of the effective one-electron potential for different number of electrons Q added to the system. The potential is shown as function of the ρ-coordinate for $z = 0$. The dashed horizontal line represents the vacuum level. The vertical blue line denotes the disk boundary R. b) Dependence of the energy of the Fermi level on the number of electrons Q added to the system, as obtained from the DFT calculations. The energy is measured with respect to the vacuum level. The line shows the analytical fit by a linear dependence.

in Fig. 2a reflects the z-quantization of the electron motion, while the density oscillations (Friedel oscillations) in Fig. 2b originate from the reflection at the disck boundary $\rho = R$ of the electron waves propagating parallel to the nanodisk surface.

B. Charged system

Electron doping of the nanodisk creates a repulsive electrostatic potential that increases the energy of the bottom of the potential well confining the valence electrons and thus reduces its depth so that the change of the potential at metal vacuum interface becomes more gradual. This is shown in Fig. 3a for different number Q of electrons ($Q = 4$, 8, 12, 16, 20) added to initially neutral system. The electrical charge of the nanodisk is thus $(-Q)$ in atomic units. Based in simple considerations, and assuming an homogeneous charging of the infinitely narrow nanodisk, an additional potential acting on the electrons at the disk center is given by $V_Q = 2Q/R$. Accordingly, one can expect the shift of the energy of the Fermi level E_F with Q as:

$$E_F^Q = -\Phi + 2Q/R, \tag{12}$$

It follows from Fig. 3a, that the change of the Fermi energy calculated with DFT indeed linearly depends on Q. From the linear fit to the DFT data, we obtain $E_F^Q \sim 0.46Q$ [eV], while Eq. (12) predicts a faster change, $E_F^Q \sim 0.67Q$ [eV]. This difference is because the extra-charges are partially expelled to the disc circumference as we discuss in detail below. At the moment, to keep the qualitative discussion simple, we will use the analytical dependence given by Eq. (12).

The negative charging rises the Fermi level and decreases the work function of the nanodisk until a charging value where the system becomes unstable. For a charge doping above the critical value $Q \geq Q_{\rm cr} = \Phi\, R/2$, the Fermi level is promoted above the vacuum level, $E_F^Q \geq 0$. In this situation the electrons can escape from the nanodisk through the potential barrier at the metal/vacuum interface so that the extra charge would relax to the critical value[83]. For a neutral nanostructure with $N_e = \pi h R^2 n_0$ electrons, $Q_{\rm cr}/N_e \sim 1/R$, i.e. the larger is the nanodisk, the less (in relative terms) charge doping is possible. In the present case, however, the reduced dimensionality of the system allows higher doping rates when compared to 3D metal structures[83] with analogous electron density, where $Q_{\rm cr}/N_e \sim 1/R^2$.

In Fig. 4 we analyse the electron density change when $Q = 4, 8, 12, 16, 20$ electrons are added to the initially neutral disk. Note that for $Q > 6$, the Fermi level of the system is promoted above the vacuum level (see Fig. 3) so that *a priori* the extra charge above this value will leave the system. However, the decay rates via electron tunneling from the metal potential well into vacuum[83] are very low for charges up to $Q = 20$. This allows to converge the DFT calculations of the charged nanodisks and perform the TDDFT studies of their plasmon dynamics presented below.

For a 3D metallic object the charge neutrality in the bulk has to be preserved and additional charges are accumulated in the surface layer[83]. In the current 2D structure, addition of Q extra electrons affects the charge distribution over the entire nanodisk. This effect can be observed in Fig. 4a, where the DFT results of the electron density change $\Delta n_Q(\rho)$ are shown as a function of the radial coordinate ρ. The Δn_Q is defined as $\Delta n_Q(\rho) = \int [n_Q(\rho, z) - n_0(\rho, z)]\, dz$, where $n_Q(\rho, z)$ and $n_0(\rho, z)$ are the electron densities of the charged and neutral nanodisk, respectively. The z-integration allows a comparison with the surface charge density of a pure 2D system with zero height. Aside from the Friedel oscillations, $\Delta n_Q(\rho)$ generally grows over the entire $0 \leq \rho \leq R$

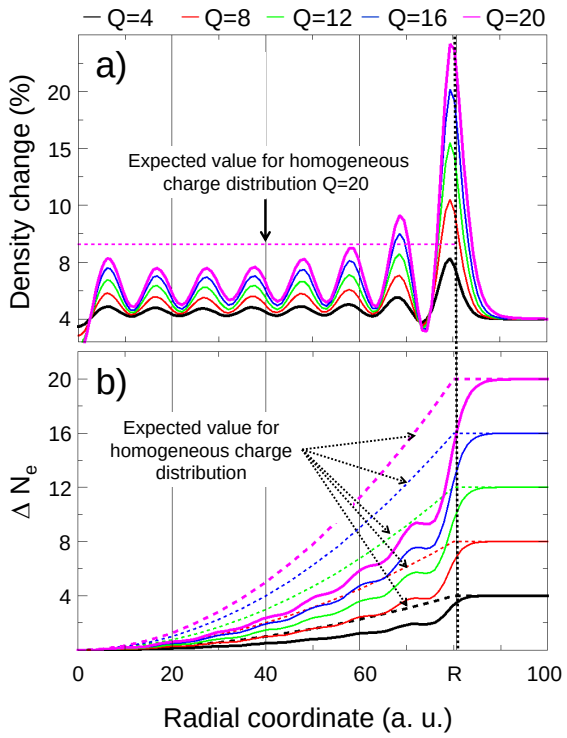

FIG. 4. Analysis of the electron density change of the nanodisk induced by negative charging. Different colors are used for results obtained with different number of electrons Q (electron charge) added to the neutral system as indicated at the top of the figure. a) DFT results for the density change. The z-integrated change of the electron density $\Delta n_Q(\rho) = \int [n_Q(\rho,z) - n_0(\rho,z)]\, dz$ is shown as function of the radial ρ-coordinate. Horizontal dashed line indicates the value of Δn expected for Q=20 in the case of an homogeneous distribution of charges over the disk. b) Number of additional electrons N_e inside a cylinder of radius ρ, concentric to the nanodisk of radious R. Dashed lines indicate the analytical dependence obtained for an homogeneous charge distribution. The vertical dashed lines in both panels of the figure denote the nanodisk boundary R.

range as Q increases, as observed in Fig. 4a. However, inside the disk the charge doping is nearly twice smaller than what would be expected for an homogeneous distribution of the extra-electrons, while the proximity of the disk boundary R shows a larger accumulation of the extra charge. The charge accumulation at R results in an electron density spill out in vacuum, which increases with Q. Similar results have been reported in self consistent calculations for graphene nanostructures[53,84], albeit tight binding or classical descriptions in that case prevent the spill out effect to be revealed.

The above conclusions are further supported by the results in Fig. 4b, where we show the change of the total number of electrons $\Delta N_e(\rho)$ inside a disk of radius ρ, i.e. the distribution of the extra electrons in concentric disks of progressively larger size. This quantity is defined as $\Delta N_e(\rho) = 2\pi \int_0^\rho \Delta n(\rho')\rho' d\rho'$. In the case of an homogeneous increase of the electron density upon doping, the $\Delta N_e(\rho)$ would adopt the values $\Delta N_e^{\rm hm}(\rho) = Q\rho^2/R^2$ for $\rho \le R$, and $\Delta N_e^{\rm hm}(\rho) = Q$ for $R \le \rho$, as indicated by dashed lines in Fig. 4b. In the self-consistent DFT calculations because of the electron-electron repulsion the electron density change is not homogeneous over the nanodisk. Approximately half of the additional charges are expelled into a surface region of ≈ 5 Å width around the nanodisk circumference of radius R, extending into the vacuum region.

The accumulation of about half of the extra charges within the ring of radius R also explains the slower increase of the Fermi energy with Q obtained from the DFT study when compared with the analytical prediction given by Eq. (12). In deriving Eq. (12) we assumed a uniformly charged disk while self-consistent calculation shows that half of the additional charge is accumulated at the disc circumference. The mean value between the potential created at the coordinate origin by the uniformly charged disk, $2Q/R$, and that created by a ring, Q/R, results in a value of $E_F^Q \approx 0.5Q$ [eV], i.e. very close to the relationship $E_F^Q \sim 0.46Q$ [eV], derived from the fit to the DFT data.

IV. OPTICAL RESPONSE OF CHARGED MONOATOMIC METALLIC NANODISKS

A. Excitation by a plane wave

We analyse in this sub-section the optical response of a charged monoatomically thin metallic nanodisk induced by an incoming linearly polarized plane wave with different directions of polarization. One might expect that for a 1ML-thick nanodisk the in-plane optical response could be similar when calculated within quantum and classical frameworks owing to the large lateral size that shows a pseudo-continuum of electronic states propagating in the ρ-direction. In contrast, the optical response of the system to a z-polarized electromagnetic wave should be strongly affected by the quantum-size effect because of the confinement of the electron motion in z-direction.

In Fig. 5 we present the absorption spectra calculated for neutral and negatively charged sodium nanodisks as a response to an incoming electromagnetic plane wave polarized parallel to the disk plane (in-plane excitation). We start our analysis with a case of the neutral nanodisk. The absorption spectrum in this case is very similar in both classical and quantum calculations. It is dominated by the excitation of an in-plane dipolar plasmon mode (DP) at the frequency $\omega_{\rm DP} = 0.9$ eV. The corresponding induced charge density profile, $-\Delta n_{\rm DP}$, is shown in the $(x, y, z = 0)$ equatorial plane of the nanodisk in the insert of Fig. 5b. The induced electron density $\Delta n_{\rm DP}(\mathbf{r}) = n(\mathbf{r}, t^*) - n(\mathbf{r}, t = 0)$ is obtained from the time-dependent electron density $n(\mathbf{r}, t)$ by exposing the system to the linearly z-polarized electromagnetic wave with frequency

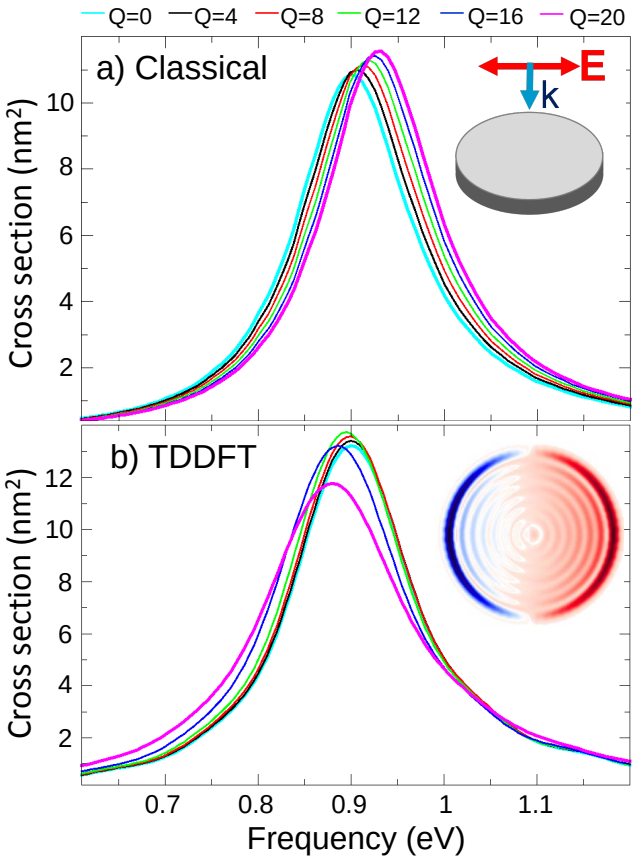

FIG. 5. Absorption spectra of neutral and negatively charged monoatomic metallic nanodisks obtained with classical electromagnetic calculations [panel a)], and with quantum TDDFT calculations [panel b)]. The incoming field is a plane wave incident along the disk symmetry axis and polarized parallel to the disk surface, as shown in the inset of panel a). Different colors are used for results obtained with a different number of extra electrons Q (electron charge) added to the neutral system, as indicated on the top of the figure. Results are shown as a function of the frequency of the incident radiation. The insert of panel b) shows the induced charge density calculated with TDDFT at the equatorial plane of the neutral disk for the frequency of the dipolar plasmon mode $\omega_{\rm DP} = 0.9$ eV. The negative (positive) values of the induced charge density are shown with blue (red) color.

$\omega = \omega_{\rm DP}$. The instant of time t^* corresponds to the maximum induced dipole.

Importantly, when Q electrons are added to the system, the change of the absorption spectra predicted by the classical theory, is not confirmed by the TDDFT calculations even qualitatively. Indeed, for the 2D-systems it is commonly assumed that the extra charge is homogeneously distributed over the nanoobject[26–28,47–51], so that the plasmon frequency changes as $\Delta w_p/w_p = 0.5Q/N_e$. Thus, within this assumption, in the classical calculations the plasmon modes experience a *blue-shift* with increasing Q as shown in Fig. 5a as has been also reported in the literature[51]. Observe, that in a classical picture even a nonhomogeneous doping would lead to the blue shift of the plasmon mode because the electron density would experience an overall increase.

In the optical response obtained from the quantum calculations, however, the electron doping affects both the energy and the width of the plasmon resonance in a very moderate way with a small, but visible *red shift* of the plasmon frequency. The redshift of the plasmon resonance with increasing number of extra electrons added to initially neutral system is related to the spill out of the electron density outside the disk boundaries at R. Since the DP induced charges reside mainly at the external circumference of the disk [see inset in Fig. 5b], the boundary effects mainly affect this plasmon mode. The density spill out increases with increasing Q. This leads to the red shift of the DP frequency. This effect of charging is well documented in the cluster physics. In addition to the red shift of the plasmon resonance for the negatively charged clusters, it is shown that the contraction of the electron density (reduced spill-out) for the positively charged clusters leads to the blue shift of the plasmon resonance[85–90]. On the formal level, the shift of the plasmon resonance of the nanoobject with electron addition (removal) can be related to the change of the position of the plasmon induced charges with respect to the metal/vacuum interface. This is the same physical parameter that controls cluster size dependence of the energy of the dipolar plasmon resonance[35–37,83].

It follows from the present TDDFT data that the spill out compensates and even overrides the effect of the overall increase of electron density and thus of ω_p. The classical theory with sharp boundaries does not account for the exponential tail of the electron wave functions in the vacuum region so that it cannot properly reproduce the quantum results. Since accumulation of the extra-charges at the circumference of the nanodisk is an electrostatic effect linked with repulsive electron-electron interactions, we expect it to be qualitatively the same for free-electron metal nanodisk as addressed here or for the nanodisk made of the noble metal (Au, Ag). In this later case the increased spill out of the charge density towards the vacuum should also lead to the slight red shift of $\omega_{\rm DP}$ with electron doping, as has been reported in 3D spherical metallic nanoparticles[83].

In contrast to the in-plane optical response described above, for an incident field polarized perpendicular to the plane of the disk, the TDDFT calculations reveal that the polarizability of the system $\alpha_z(\omega)$ and thus the absorption cross-section $\sigma_z(\omega)$ are strongly affected by the electron doping Q. The classical and quantum calculations for the case of z-polarized incidence are shown respectively in Fig. 6a) and in Fig. 6b). Similar to the other systems with pronounced quantization effects such as molecules[30], narrow shells[33,60], metal slabs[34] or monoatomic wires[91–93], in this polarization direction the optical response reflects transitions between the occupied and unoccupied KS orbitals derived by the z-quantization of the electron motion. Obviously, such a

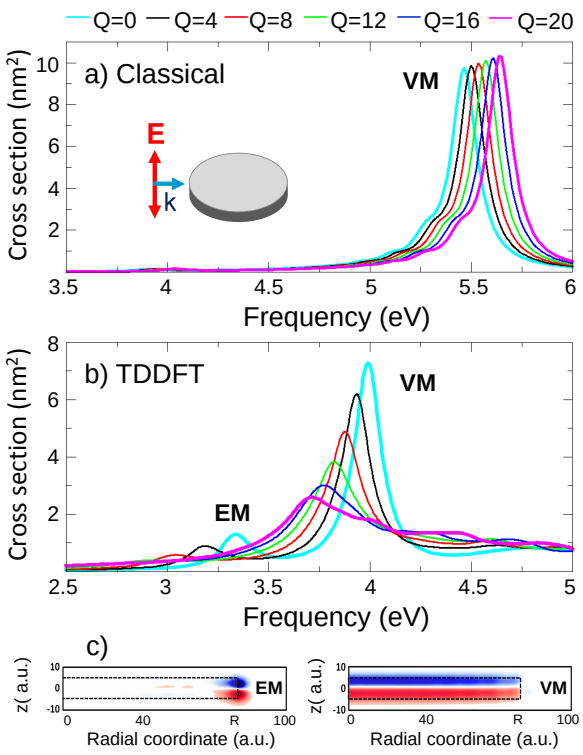

FIG. 6. Absorption spectra of neutral and negatively charged monoatomic metallic nanodisks obtained with classical electromagnetic calculations [panel a)], and with quantum TDDFT calculations [panel b)]. The incoming field is a z-polarized plane wave as shown in the inset of panel a). Different colors are used for results obtained with different number of electrons Q (electron charge) added to the neutral system, as indicated at the top of the figure. Results are shown as a function of the frequency of the incident radiation. c) Induced charge densities calculated with TDDFT for a neutral nanodisk at the $(x = 0, y, z)$ plane perpendicular to the surface of the nanodisk for the edge mode (EM) to the left, and for the vertical mode (VM) to the right. The negative (positive) values of the charge density are shown with blue (red) color.

situation involves a strong quantum character and cannot be captured within a classical electromagnetic description. The main resonance in the absorption spectrum (vertical mode, VM) is associated with the excitation of the transition between the orbitals with symmetric (occupied) and antisymmetric (empty) character in z-dependence so that the opposite charges are located at the top and bottom surfaces of the nanodisk [see right panel of Fig. 6c]. The VM has a dipolar strength similar to the in-plane dipolar plasmon mode and it appears in classical calculations close to the bulk plasmon frequency [Fig. 6a][94], while in the TDDFT results, the VM is at $\omega_{VM} = 3.99$ eV for the $Q = 0$-case [Fig. 6b].

Along with the VM resonance, in the TDDFT calculations for the $Q = 0$ -case we also find an edge mode (EM) at $\omega_{EM} = 3.34$ eV [see the left panel of Fig. 6c]. The EM arises from the ρ-coordinate dependence of the effective one-electron potential well confining the electron motion in z-direction, as has been discussed for the case of the transversal edge mode found for the monoatomic nanowires[91,92]. Similar to the VM, the EM also posses a dipolar character with induced charge density antisymmetric in z. However, while the VM is associated with induced charge density extending over entire top and bottom surface planes, the EM is localised at the disc circumference. Observe that both VM and EM posses axial symmetry. This later property of the present EM with no nodal structure in angular dependence with φ makes it quite different from the classically attainable plasmons propagating along the edges of the nanostructures[20,23–25], or multipolar plasmons in metallic nanodisks[73]. Interestingly, both have been also shown to obey the same dispersion relation[95]. As we mentioned above the physics underlying the formation of the EM in the present case is similar to the one discussed for the monoatomic nanowires[91–93], and it can not be retrieved in the classical calculations.

As the nanosdisk is negatively charged, the classical calculations predict a *blue shift* of the spectral features because of the overall increase of electron density and thus of the bulk plasma frequency w_p in the Drude dielectric function. This is analogous to the previously described case of the in-plane polarized light. The TDDFT study reveals a completely opposite trend. As the disk is negatively charged, the potential well confining the electrons within the metal becomes shallower [see Fig. 3a] and the energy difference between KS orbitals describing the vertical z-confinement decreases. The features in the absorption spectra (VM and EM) display a pronounced *red shift* with increasing Q. Because of the charge accumulation at the disc circumference the edge mode appears most sensitive to electron doping. Thus, in contrast to the in-plane dipolar plasmon, it is found here that the optical response in the out-of-plane (vertical) direction of a thin metallic nanodisk can be efficiently controlled by charge injection.

We obtained that adding $Q = 4$ extra electrons to the initially neutral nanodisk, i.e. changing the total number of the electrons by 1.3% only, results in a 60 meV red-shift of the VM frequency and 150 meV red-shift of the EM frequency. However, while the general trend obtained here should be robust, the efficiency of this control mechanism is rather difficult to predict in practical situations where 2D metal systems are usually supported over other materials. This is because the potential confining electrons inside the metal disk, and the evolution of this potential with external charging should be dependent on the specific properties of the interfaces.

In closing this subsection, a remark is in order with respect to the widths of the spectral features in optical response. For the plane wave excitation with incoming field polarized parallel or perpendicular to the surface of the nanodisk, the electron doping Q leads to the broadening of the DP mode (Fig. 5) and of the EM and VM (Fig. 6).

Similar results have been obtained for the 3D spherical clusters[83]. The increase of the width corresponds to the faster decay of the excitation by hot electron production and its eventual emission into the vacuum[86,96]. Indeed, increasing the negative charge of the nanodisk lowers the depth of the potential well confining the electrons as seen in Fig. 3.

B. Excitation by a point dipole

While the excitation of the nanodisk system by an incident electromagnetic plane wave discussed above allows to address plasmon modes with dipolar character, the eventual dependence of dark breathing plasmon modes[73,95] on the electronic charge of the nanodisk is also of interest. Breathing plasmon modes are accessible for instance in electron energy loss spectroscopy, or when considering the excitation by a point dipole, as we use here. These are standing electron charge density waves due to the confinement of radially propagating plasmons (cylindrical waves)[97] scattered back by the radial disk boundary. If relevant values of plasmon energy dependence were found in this case, the frequency change of breathing plasmon modes with electron doping could open the possibility to actively control the coupling of a quantum emitter to a flat nanodisk antenna[98], and thus the decay of the former. Since the breathing modes are non-radiative this is predominantly the non-radiative contribution to the total decay rate of the nanoemitter[79,80] that might be affected in this way.

For a z-oriented dipole located at the symmetry axis of the nanodisk, only the $m = 0$ modes are excited. Here m stands for the azimuthal quantum number defining the $\exp(im\varphi)$ dependence of the plasmon fields. These are the "dark" plasmon modes with zero dipole moment. According to the symmetric or antisymmetric distribution of the plasmon induced charge density at the opposite top and bottom surfaces of the disk (z-coordinate), two branches of modes exist: tangencial and normal[94]. Since in our case the typical plasmon wave vectors $q \simeq 1/R$ are such that $\omega_p \ll cq$, we can use the nonretarded approximation for the dispersion of the plasmon modes, which is consistent with the TDDFT procedure used here. The dispersion of the tangencial (symmetric) plasmons in a metallic thin film is given by[94]

$$\omega_- = \frac{\omega_p}{\sqrt{2}}\left(1 - e^{-hq}\right)^{1/2} \approx \frac{\omega_p}{\sqrt{2}}\sqrt{hq},\ hq \ll 1, \qquad (13)$$

and the dispersion of the normal (antisymmetric) plasmons is given by

$$\omega_+ = \frac{\omega_p}{\sqrt{2}}\left(1 + e^{-hq}\right)^{1/2} \approx \frac{\omega_p}{\sqrt{2}}\sqrt{2 - hq},\ hq \ll 1. \quad (14)$$

The wave vectors q are quantized in our nanodisk system because of the reflection at the disk boundary at R: $Rq_\ell = \pi\ell + \phi_\ell$ leading to a discrete spectrum of breathing plasmon modes. Here, $\ell = 1, 2, ...$ is the radial quantum number, and ϕ_ℓ is the phase of the reflection at the boundary.

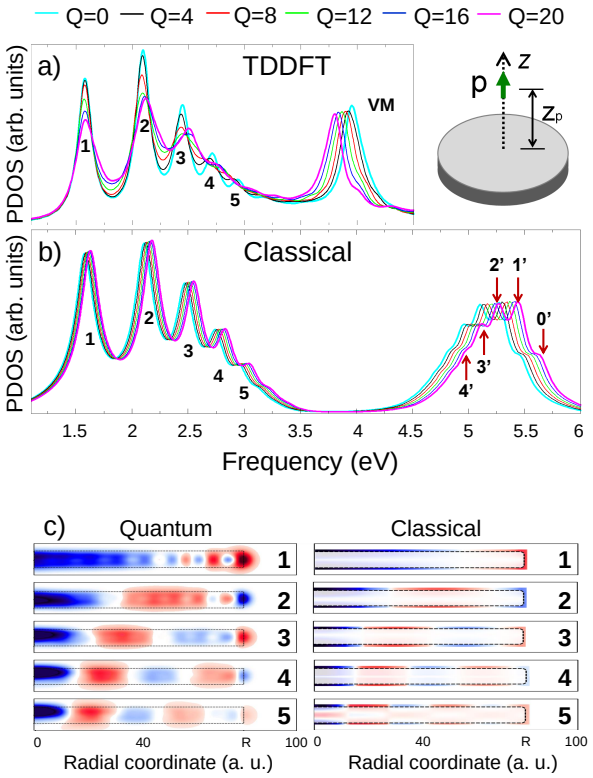

FIG. 7. Projected density of electromagnetic states, PDOS, as obtained from TDDFT (a) and classical Drude (b) calculations for a z-oriented point dipole placed at the symmetry axis of the disk, 1 nm above the nanodisk surface (see the sketch). Results are shown as a function of the frequency of the dipole emitter. Different colors are used for results obtained with a different number of electrons Q (electron charge) added to the neutral system, as indicated at the top of the figure. The symmetric and antisymmetric plasmon modes are labelled with their radial quantum number. We use labels with "prime" for the antisymmetric modes to distinguish between the two types of excitations. c) Induced charge densities calculated with TDDFT and classical Drude approach corresponding to the symmetric plasmon modes of a neutral monoatomic disk. Results are shown in the $(x = 0, y, z)$ plane perpendicular to the surface. The modes are labelled as in panel a) of the figure. The negative (positive) values of the electron density are shown in blue (red) color.

To study the dependence of the breathing plasmon modes on electron doping we have calculated the projected density of electromagnetic states (PDOS) of the nanodisk $\mathfrak{N}_{\rm ns}(z_p, \omega)$ given by Eq. (10) by placing a unit point dipole $\mathbf{p} = \hat{e}_z$ at position $z_p = 1$ nm on the symmetry z-axis. In Fig. 7 we compare classical and TDDFT results of $\mathfrak{N}_{\rm ns}(z_p, \omega)$ obtained for the neutral and negatively charged nanodisks. To improve the contrast of the high-frequency modes only $Im\{\hat{e}_z \mathbf{E}_{\rm ns}(z_p, \omega)\}$ is shown in Fig. 7a) and Fig. 7b), i.e. the $1/\omega$ multiplier is omitted.

The low-energy part of the PDOS reveals an in-plane optical response without excitation of the electron transitions between lowest occupied (symmetric) and higher energy (antisymmetric) states confined by the metal potential well in z-direction. Similar to the in-plane dipolar plasmon excitation, the TDDFT results for the breathing modes with symmetric character in the neutral ($Q = 0$) case are well reproduced with classical simulations (modes frequency and width). Up to five plasmon modes can be clearly distinguished in the spectra. These modes can be labelled according to their radial quantum number ℓ, and have a distribution of frequencies of $\omega_{-,1} = 1.59$ eV, $\omega_{-,2} = 2.10$ eV, $\omega_{-,3} = 2.45$ eV, $\omega_{-,4} = 2.72$ eV, and $\omega_{-,5} = 2.95$ eV, as obtained with TDDFT. The energy dispersion of the symmetric breathing modes is well described by the dependence $\omega^2_{-,\ell} \propto \ell$, as follows from Eq. (13), and assuming $q_\ell = [\pi\ell + \phi]/R$. This indicates that the reflection phase changes only weakly within the considered energy window ($\phi_\ell \approx \phi$, $\ell = 1, 2, 3, 4, 5$). The above assignment of modes is further confirmed by the corresponding induced charge densities shown in Fig. 7c. In the classical calculations to the right of Fig. 7c, the induced surface charge density at the boundaries is obtained from the difference in the components of the fields perpendicular to the metal surface.

As the nanodisk is negatively charged, classical calculations predict a blue shift of the plasmon modes through the increase of the electron density and thus of ω_p (see Eq. (13)). The quantum calculations also indicate a blue shift and broadening of the symmetric breathing modes. Both effects are more pronounced for the states with higher frequencies. As follows from the static DFT results, with an increasing number of additional electrons Q the overall electron density increases within the nanodisk, even though to lesser extent than that expected for the homogeneous charging (see Fig. 4). The electron density increase leads to the blue shift of the energies of the in-plane plasmons propagating in ρ-direction. However, this tentative explanation has to be considered with care, as the phase shift ϕ associated with the plasmon wave reflection at the nanodisk boundary is *a priori* also charge dependent. The boundary effect might also explain the broadening of the plasmon modes[99] as has been also observed in charged spherical metal clusters[83]. It is worthwhile mentioning that the frequency shift attainable for the symmetric breathing modes is moderate since the charging Q itself is limited.

At higher frequencies, along with the vertical mode (VM), the breathing plasmon modes associated with normal (antisymmetric) plasmons are excited by the point dipole located above the surface of the nanodisk. As we already discussed for z-polarized plane wave excitation, the VM corresponds to a distribution of opposite charges at the upper and lower surfaces of the nanodisk with no nodal structure in the ρ-direction. Within the current definition of the breathing modes, this mode can be formally denoted as the $\ell = 0'$ antisymmetric mode. We use labels with "prime" for the antisymmetric modes to distinguish between the two types of excitations. The $\ell \geq 1'$ antisymmetric modes form a dense energy series with their frequency decreasing with increasing q and thus ℓ, as follows from Eq. (14). These modes are well resolved in classical calculations shown in Fig. 7b where the VM has an energy close to ω_p.

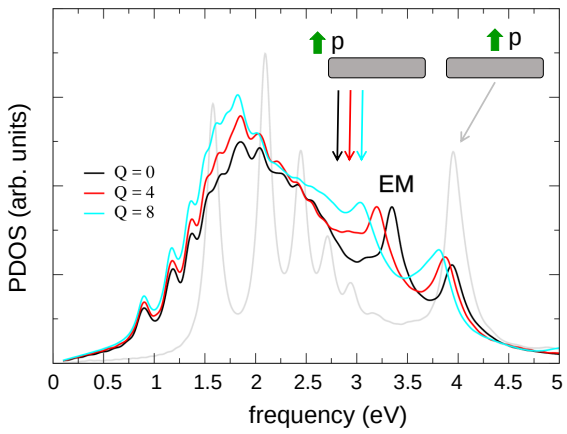

FIG. 8. Projected density of electromagnetic states, PDOS, obtained with TDDFT for a neutral nanodisk $Q = 0$ and nanodisk externally charged by adding $Q = 4$, and $Q = 8$ electrons. Two locations of the z-oriented point dipole are considered, as sketched in the insets. For the spectrum in gray the dipole is placed at the symmetry axis of the $Q = 0$ disk ($x = y = 0$, $z = 1$ nm). For the spectra in black ($Q = 0$), red ($Q = 4$), and cyan ($Q = 8$) the dipole is placed outside the disk, close to its edge ($x = R+1$ nm, $y = 0$, and $z = 0.25$ nm). In the latter case the result is scaled by a factor of 2. The origin of coordinates is at the centre of the nanodisk. The quantity $Im\{\hat{e}_z \mathbf{E}_{\rm ns}(z_p, \omega)\}$ is shown in arbitrary units as a function of the frequency ω of the dipole. EM stands for the nanodisk edge mode.

The excitation of an antisymmetric distribution of plasmon induced charge density at opposite surfaces of the nanodisk requires transitions between lowest occupied (symmetric) and higher unoccupied (antisymmetric) states, confined by the metal potential well in the z-direction. This situation is thus sensitive to the details of the electronic structure and this is the reason why the series of antisymmetric modes (associated to the VM) shows a lower energy in the TDDFT results as compared to those in the classical calculations (compare the energy of VM and the series of 0', 1', 2', 3' and 4' in Fig. 7a and Fig. 7b respectively). In difference to classical Drude results, the individual peaks in the PDOS associated with these modes are not resolved in the quantum calculations. However, the analysis of the induced electron density calculated with TDDFT over the frequency range around $\omega_{\rm VM}$ (not shown here) indicates that the feature appearing as a single resonance in the PDOS is, in fact, formed by several overlapping resonances. Each of these "hidden" resonances is characterised by a specific induced density profile, antisymmetric in z with a nodal struc-

ture developing along the ρ coordinate as the frequency is decreasing from $\omega_{\rm VM}$.

When external electrons are added to initially neutral nanodisk, the frequency of the resonance in the PDOS calculated with TDDFT and associated with the VM [Fig. 7a)] experiences a strong red shift with electron doping. Obviously, because of the same underlying physics this result is consistent with VM shift obtained in the TDDFT for the excitation with a z-polarized plane wave [Fig. 6b)]. The antisymmetric breathing modes pinned to VM are also strongly red shifted. This quantum behaviour is not reproduced in the classical electromagnetic calculations which predict that *all* the modes are blue shifted with increasing Q, irrespective of their character.

For a point dipole positioned at the nanodisk symmetry axis, the EM is weakly excited and cannot be resolved in the PDOS. As the point dipole position is shifted from the symmetry axis at $\rho = 0$ towards the edge of the nanodisk, the efficiency of the EM excitation and thus the the intensity of the associated peak in the PDOS increases. This effect can be clearly observed in the TDDFT data shown in Fig. 8 for the neutral and negatively charged nanodisks. When the point dipole located close to the edge of the nanodisk, the EM clearly emerges in the PDOS. In this situation, the excitation of the in-plane dipolar mode, multipolar modes, as well as the breathing symmetric plasmon modes characterised by the different (m, j) quantum numbers[95], leads to a broad structure in the PDOS below 3 eV. Consistently with results obtained with TDDFT for the excitation with a z-polarized plane wave [Fig. 6b] the resonance in PDOS associate with plasmonic EM strongly red shifts with electron doping. The strong sensitivity of the EM to the electronic charge of the nanodisk thus offers an interesting possibility to exploit the active control of the decay rate of quantum emitters coupled to monoatomic metallic nanoantennas.

V. CONCLUSIONS AND OUTLOOK

We have studied the optical absorption cross section and the electromagnetic density of states of charged and neutral 2D metallic nanostructures using quantum approaches based on the density functional theory and time-dependent density functional theory, as well as using classical approaches. With an example of a monolayer-thick free-electron metallic nanodisk in vacuum, we have shown how quantum effects alter the optical response of a 2D metallic nanoantenna, the excitation of its bright and dark plasmon modes, and the dependence of the optical response on electron doping.

We have demonstrated that optical excitations in the *neutral* system and their sensitivity to quantum effects can be understood from the profile of the associated induced charge density.

The dipolar plasmon mode excited by incident electromagnetic radiation polarised parallel to the disk plane, and the symmetric breathing dark plasmon modes excited by a point dipole located at the disk axis are characterized by symmetric distributions of the plasmon induced charge density at both top and bottom surfaces of the nanodisk. The optical response in this case involves nearly free electron motion in the lateral direction and thus the quantum and classical results for the neutral system are very close to each other.

The optical response associated with antisymmetric distributions of the charge density induced by an external potential at the top and bottom surfaces of the nanodisk requires hybridization between symmetric and antisymmetric electronic orbitals describing a quantized electron motion strongly confined in the direction perpendicular to the disk plane. The quantum results in this case cannot be retrieved classically. Thus, for the dipolar transitions excited by an incident electromagnetic radiation polarised perpendicular to the disc plane, or for the antisymmetric breathing plasmon modes, the classical theory maximizes the optical response and electromagnetic density of states close to the bulk plasmon frequency. In contrast, quantum results are determined by the excitation energy between the z-quantized states.

Our quantum calculations reveal the excitation of a plasmon edge mode localized at the disk boundary. This mode is axially symmetric and it is characterized by an antisymmetric charge density distribution induced at the top and bottom surfaces of the nanodisk. Different from the propagating edge plasmons discussed classically[20,23–25,73,95], the edge mode of the nanodisk found here stems from lateral coordinate dependence of the confining potential and it is similar to the transverse edge mode reported in quantum calculations of the monoatomic wires[91–93]

For nanodisks *negatively charged* by electron doping several quantum effects are important:

- The energy of the Fermi level increases so that above a certain critical charge, the system becomes unstable. This limits the range of the possible electron doping.
- The metal potential well becomes less attractive and the excitation energy between z-quantized states is reduced with increase of the number of additional electrons.
- The additional charges are distributed nonhomogeneously over the 2D object. The charge accumulation at the circumference of the disk leads to the spill out of the electron density outside the disk which increases with increasing electronic charge Q.

These quantum effects lead to quantitative and even qualitative differences between quantum and classical results for negatively charged nanodisks. The classical theory predicts a *blue shift* of all the spectral features in the optical response because of the overall increase of the electron density. While this is confirmed by the TDDFT calculations only for the in-plane symmetric

breathing modes, the frequency of the in-plane dipolar plasmon mode with symmetric character appears nearly unaffected by negative charge doping. This is because the electron spill out effect compensates in this case the overall increase of the electron density. As to the optical excitations associated with antisymmetric induced charge density, the TDDFT calculations show a charging effect opposite to that predicted classically. The features in the optical response are *red shifted* with increasing Q because of the decreasing energy spacing between z-quantized states.

Our results indicate that the optical absorption for incident light polarised perpendicular to the plane of the nanodisk and the plasmon edge mode are the most sensitive to negative charging of the nanoobject. In particular, the frequency shift of the edge plasmon mode with negative charging could allow an efficient control of the optical absorption and of the coupling between quantum emitters and 2D metallic nanoantennas. The robust effects revealed here can thus be used in control of single photon emitters and design of optically active devices.

ACKNOWLEDGMENTS

J.A. and M.Z. acknowledges support from the Spanish Ministry of Economy, Industry and Competitiveness through project FIS2016-80174-P, as well as support from NIST grant nr. 70NANB15H32 of the US Department of Commerce. A.K.K acknowledges financial support from the project FIS2016-76617-P of MINECO. M. Z. also acknowledges the hospitality of the Institute des Sciences Moléculaires d'Orsay.

* andrei.borissov@u-psud.fr

[1] D. K. Gramotnev and S. I. Bozhevolnyi, Nat. Photonics **4**, 83 (2010).
[2] J. N. Anker and W. P. Hall, Nat. Materials **7**, 442 (2008).
[3] A. Kinkhabwala, Z. Yu, S. Fan, Y. Avlasevich, K. Müllen and W. E. Moerner, Nat. Photonics **3**, 654 (2009).
[4] L. Novotny and N. van Hulst, Nat. Photonics **5**, 83 (2011).
[5] J. P. Camden, J. A. Dieringer, J. Zhao and R. P. Van Duyne, Acc. Chem. Res. **41**, 1653 (2008).
[6] H. Chen, G. C. Schatz and M. A. Ratner, Rep. Prog. Phys. **75**, 096402 (2012).
[7] K. M. Mayer and J. H. Hafner, Chem. Rev. **111**, (6) 3828 (2011).
[8] J. Langer, S. Novikov and L. M. Liz-Marzán, Nanotechnology **26**, 322001 (2015).
[9] G. Baffou and R. Quidant, Chem. Soc. Rev. **43**, 3898 (2014).
[10] C. Clavero, Nat. Photonics **8**, 95 (2014).
[11] M. Kauranen and A. V. Zayats, Nat. Photonics **6**, 737 (2012).
[12] H. Aouani, M. Rahmani, M. Navarro-Cía, S. A. Maier Nature Nanotechnology **9**, 290 (2014).
[13] H. A. Atwater and A. Polman, Nat. Materials **9**, 205 (2010).
[14] V. J. Sorger, R. F. Oulton, R. -M. Ma and X. Zhang, MRS Bulletin **37**, 728 (2012).
[15] J. Ho, J. Tatebayashi, S. Sergent, Ch. F. Fong, Y. Ota, S. Iwamoto, Y. Arakawa, Nano Lett. **16**, 2845 (2016).
[16] E. C. Garnett, W. Cai, J. J. Cha, F. Mahmood, S. T. Connor, M. Greyson Christoforo, Y. Cui, M. D. McGehee, M. L. Brongersma, Nature Materials **11**, 241 (2012).
[17] M. Mayer, L. Scarabelli, K. March, T. Altantzis, M. Tebbe, M. Kociak, S. Bals, F. J. García de Abajo, A. Fery, L. M. Liz-Marzán, Nano Lett. **15**, 5427 (2015).
[18] Y. Fang, Z. Li, Y. Huang, S. Zhang, P. Nordlander, N. J. Halas, H. Xu, Nano Lett. **10**, 1950 (2010).
[19] A. L. Fetter Phys. Rev. B **33**, 5221 (1986).
[20] L. Gu, W. Sigle, C. T. Koch, B. Ögüt, P. A. van Aken, N. Talebi, R. Vogelgesang, J. Mu, X. Wen, J. Mao, Phys. Rev. B **83**, 195433 (2011).
[21] F.-Ph. Schmidt, H. Ditlbacher, U. Hohenester, A. Hohenau, F. Hofer, J. R. Krenn, Nature Communications **5**, 3604 (2014).
[22] W. Wang, P. Apell, J. Kinaret, Phys. Rev. B **84**, 085423 (2011).
[23] T. Ando, A. B. Fowler, F. Stern Rev. Mod. Phys. **54**, 437 (1982).
[24] Z. Fei, M. D. Goldflam, J.-S. Wu, S. Dai, M. Wagner, A. S. McLeod, M. K. Liu, K. W. Post, S. Zhu, G. C. A. M. Janssen, M. M. Fogler and D. N. Basov, Nano Lett. **15**, 8271 (2015).
[25] A. Y. Nikitin, P. Alonso-González, S. Vélez, S. Mastel, A. Centeno, A. Pesquera, A. Zurutuza, F. Casanova, L. E. Hueso, F. H. L. Koppens and R. Hillenbrand, Nat. Photonics, **10**, 239 (2016).
[26] F. Wang, Y. Zhang, C. Tian, C. Girit, A. Zettl, M. Crommie, Y. R. Shen, **320**, 2006 (2008).
[27] Z. Fei, A. S. Rodin, G. O. Andreev, W. Bao, A. S. McLeod, M. Wagner, L. M. Zhang, Z. Zhao, M. Thiemens, G. Dominguez, M. M. Fogler, A. H. Castro Neto, C. N. Lau, F. Keilmann, D. N. Basov, Nature 487, 82 (2012).
[28] J. Chen, M. Badioli, P. Alonso-González, S. Thongrattanasiri, F. Huth, J. Osmond, M. Spasenović, A. Centeno, A. Pesquera, P. Godignon, A. Zurutuza Elorza, N. Camara, F. J. García de Abajo, R. Hillenbrand, F. H. L. Koppens, Nature 487, 77 (2012).
[29] F. Xia, H. Wang, D. Xiao, M. Dubey, A. Ramasubramaniam, Nature Photonics 8, 899 (2014).
[30] A. Lauchner, A. E. Schlather, A. Manjavacas, Y. Cui, M. J. McClain, G. J. Stec, F. Javier García de Abajo, P. Nordlander, N. J. Halas, Nano Lett. **15**, 6208 (2015).
[31] A. J. Wilson, K. A. Willets, Ann. Rev. of Analytical Chemistry 9, 27 (2016).
[32] T. Wang, Ch. A. Nijhuis, Applied Materials Today **3**, 73 (2016).
[33] E. Prodan, P. Nordlander, N.J. Halas, Chem. Phys. Lett. **368**, 94 (2003).
[34] Z. Yuan, S. Gao, Phys. Rev. B **73**, 155411 (2006).
[35] P. Apell and A. Ljungbert, Solid State Commun. **44**, (9) 1367 (1982).
[36] A. Liebsch, Phys. Rev. B. **48**, 11317 (1993).
[37] R. C. Monreal, T. J. Antosiewicz and S. P. Apell, New

Journal of Physics **15**, 083044 (2013).
[38] J. Zuloaga, E. Prodan and P. Nordlander, Nano Lett. **9**, 887 (2009).
[39] D. C. Marinica, A. K. Kazansky, P. Nordlander, J. Aizpurua and A. G. Borisov, Nano Lett. **12**, 1333 (2012).
[40] J. A. Scholl, A. García-Etxarri, A. L. Koh, J. A. Dionne, Nano Lett. **13**, 564 (2013).
[41] G. Toscano, J. Straubel, A. Kwiatkowski, C. Rockstuhl, F. Evers, H. Xu, N. A. Mortensen, M. Wubs, Nature Communications **6**, 7132 (2015).
[42] Y.-W. Huang, H. W. H. Lee, R. Sokhoyan, R. A. Pala, K. Thyagarajan, S. Han, D. P. Tsai, H. A. Atwater, Nano Lett. **16**, 5319 (2016).
[43] C. Große, A. Kabakchiev, T. Lutz, R. Froidevaux, F. Schramm, M. Ruben, M. Etzkorn, U. Schlickum, K. Kuhnke, K. Kern, Nano Lett. **14**, 5693 (2014).
[44] A. Emboras, J. Niegemann, P. Ma, C. Haffner, A. Pedersen, M. Luisier, C. Hafner, T. Schimmel, J. Leuthold, Nano Lett. **16**, 709 (2016).
[45] D. Xiang, J. Wu, and R. Gordon Nano Lett., Article ASAP, DOI: 10.1021/acs.nanolett.7b00360 (2017).
[46] D. C. Marinica, M. Zapata, P. Nordlander, A. K. Kazansky, P. M. Echenique, J. Aizpurua, A. G. Borisov, Science Advances **1**, e1501095 (2015).
[47] K. C. Chu, C. Y. Chao, Y. F. Chen, Y. C. Wu and C. C. Chen, Appl. Phys. Lett., **89**, 103107 (2006).
[48] S. K. Dondapati, M. Ludemann, R. Müller, S. Schwieger, A. Schwemer, B. Handel, D. Kwiatkowski, M. Djiango, E. Runge and T. A. Klar, Nano Lett. **2012**, *12*, 1247 (2012).
[49] L.-H. Shao, M. Ruther, S. Linden, S. Essig, K. Busch, J. Weissmuller and M. Wegener, Advances Materials **22**, 5173 (2010).
[50] P. Mulvaney, J. Perez-Juste, M. Giersig, L. M. Liz-Marzán and C. Pecharroman, Plasmonics **1**, 61 (2006).
[51] A. Majavacas, F. J. García de Abajo, Nature Comm. **5**, 3548 (2012).
[52] F. J. García de Abajo, A. Majavacas, Faraday Discuss. **178**, 87 (2015).
[53] S. Thongrattanasiria, I. Silveiro and F. J. García de Abajo, Appl. Phys. Lett. **100**, 201105 (2012).
[54] V. V. Popov, O. V. Polischuk, T. V. Teperik, X. G. Peralta, S. J. Allen, N. J. M. Horing, M. C. Wanke, Journal of Applied Physics **94**, 3556 (2003).
[55] G. C. Dyer, G. R. Aizin, S. Preu, N. Q. Vinh, S. J. Allen, J. L. Reno, E. A. Shaner, Phys. Rev. Lett. **109**, 126803 (2012).
[56] N. D. Lang and W. Kohn, Phys. Rev. B. **3**, 1215 (1970).
[57] M. Brack, Rev. Mod. Phys. **65**, 677 (1993).
[58] M. J. Puska, R. M. Nieminen, Phys. Rev. A **47**, 1181 (1993).
[59] J. Lermé, B. Palpant, E. Cottancin, M. Pellarin, B. Prével, J. L. Vialle, M. Broyer, Phys. Rev. B **60**, 16151 (1999).
[60] E. Prodan, P. Nordlander and N. J. Hallas, Electronic structure and Optical properties of gold nanoshells. Nano Lett. **3**, (10) 1411 (2003).
[61] M. W. Knight, N. S. King, L. Liu, H. O. Everitt, P. Nordlander and N. J. Halas, ACS Nano **8**, 1 (2013).
[62] B Metzger, M. Hentschel, H. Giessen, Nano Lett. **17**, 1931 (2017).
[63] I. W. Lyo and E. W. Plummer, Phys. Rev. Lett. **60**, 1558 (1988).
[64] H. Kitamura, J. Phys.: Condens. Matter. **25**, 065505 (2013).
[65] T. V. Teperik, P. Nordlander, J. Aizpurua, and A. G. Borisov, Optics Express, **22** 27306 (2013).
[66] K. J. Savage, M. M. Hawkeye, R. Esteban, A. G. Borisov, J. Aizpurua, J. J. Baumberg, Nature **491**, 574 (2012).
[67] W. Zhu, K. B. Crozier, Nature Communications **5**, 5228 (2014).
[68] G. Hajisalem, M. S. Nezami, R. Gordon, Nano Lett. **14**, 6651 (2014).
[69] A. Sanders, R. W. Bowman, J. J. Baumberg, Scientific Reports **6**, 32988 (2016).
[70] P. Zhang, J. Feist, A. Rubio, P. García-González and F. J. García-Vidal, Phys. Rev. B **90**, 161407(R) (2014).
[71] M. Barbry, P. Koval, F. Marchesin, R. Esteban, A. G. Borisov, J. Aizpurua and D. Sánchez-Portal, Nano Lett., **15** (5), 3410 (2015).
[72] T. P. Rossi, A. Zugarramurdi, M. J. Puska, and R. M. Nieminen, Phys. Rev. Lett. **115**, 236804 (2015).
[73] F. P. Schmidt, H. Ditlbacher, U. Hohenester, A. Hohenau, F. Hofer and J. R. Krenn, Nano Lett. **12**, 5780 (2012).
[74] W. Kohn, L. J. Sham, Phys. Rev. **140**, A1133 (1965).
[75] O. Gunnarsson and B. I. Lundqvist, Phys. Rev. B. **13**, 4274 (1976).
[76] M. A. L. Marques and E. K. U. Gross, Annu. Rev. Phys. Chem. **55**, 427 (2004).
[77] R. E. Stratmann,G. E. Scuseria and M. J. Frisch. J. Chem. Phys. **109**, 8218 (1998).
[78] L. Novotny and B. Hecht, Cambridge University Press (2006).
[79] R. Carminati, J.-J. Greffet, C. Henkel, J.M. Vigoureux, Optics Communications **261**, (2) 368 (2006).
[80] R. Carminati, A. Cazé, D. Cao, F. Peragut, V. Krachmalnicoff, R. Pierrat, Y. De Wilde, Surf. Sci. Rep. **70**, 1 (2015).
[81] G. Colas des Francs and G. A. Dereux, J. Chem. Phys. **117**, (10) 4659 (2002).
[82] F. J. García de Abajo, A. Howie, Phys. Rev. B **65**, 115418 (2002).
[83] M. Zapata Herrera, J. Aizpurua, A. K. Kazansky and A. G. Borisov, Langmuir **32**, 2829 (2016).
[84] R. Yu, J. D. Cox, and F. J. García de Abajo, Phys. Rev. Lett. **117**, 123904 (2016).
[85] J. Tiggesbäumker, L. Köller and K. -H. Meiwes-Broer, Chem. Phys. Lett. **260**, 428 (1996).
[86] A. Rubio, L. C. Balbas, J. A. Alonso, Phys. Rev. B **46**, 4891 (1992).
[87] T. Reiners, H. Haberland, Phys. Rev. Lett. **77**, 2440 (1996).
[88] Ch. Schmitt, Ch. Ellert, M. Schmidt and H. Haberland, Zeitschrift für Physik D Atoms, Molecules and Clusters, **42**, 145 (1997).
[89] N. Dam, W. A. Saunders, Phys. Rev. B **46**, 4205 (1992).
[90] V. Kresin, Phys. Rev. B. **40**, 12507 (1989).
[91] J. Yan, Z. Yuan, S. Gao, Phys. Rev. Lett. **98**, 216602 (2007).
[92] J. Yan, S. Gao, Phys. Rev. B **78**, 235413 (2008).
[93] B. Gao, K. Ruud, Y. Luo, J. Chem. Phys. **137**, 194307 (2012).
[94] J. M. Pitarke, V. M. Silkin, E. V. Chulkov and P. M. Echenique, Rep. Prog. Phys. **70**, 1 (2007).
[95] F.-P. Schmidt, H. Ditlbacher, U. Hohenester, A. Hohenau, F. Hofer and J. R. Krenn, Nature Comm., **5**, 3604 (2014).
[96] A. Manjavacas, J. G. Liu, V. Kulkarni, P. Nordlander, ACS Nano **8**, 7630 (2014).
[97] S. Nerkararyan, Kh. Nerkararyan, N. Janunts, and T. Pertsch, Phys. Rev. B **82**, 245405 (2010).

[98] R. Esteban, T. V. Teperik, J. J. Greffet, Phys. Rev. Lett. **104**, 026802 (2010).
[99] J. Lermé, H. Baida, C. Bonnet, M. Broyer, E. Cottancin, A. Crut, P. Maioli, N. Del Fatti, F. Vallée, M. Pellarin, J. Phys. Chem. Lett. **1**, 2922 (2010).